Title

Hypsochromically-shifted Emission of Metal-organic Frameworks Generated through Post-synthetic Ligand Reduction

Journal

Angewandte Chemie, 135(25)

ISSN

0044-8249

Authors

Smith, Kyle T

Hunter, Kye

Chiu, Nan-Chieh

et al.

Publication Date

2023-06-19

DOI

10.1002/ange.202302123

Peer reviewed

Metal-Organic Frameworks

How to cite:
International Edition: doi.org/10.1002/anie.202302123
German Edition: doi.org/10.1002/ange.202302123

Hypsochromically-shifted Emission of Metal-organic Frameworks Generated through Post-synthetic Ligand Reduction

*Kyle T. Smith, Kye Hunter, Nan-Chieh Chiu, Hao Zhuang, Peemapat Jumrusprasert, William F. Stickle, Jeffrey A. Reimer, Tim J. Zuehlsdorff, and Kyriakos C. Stylianou**

Abstract: Luminescent materials with tunable emission are becoming increasingly desirable as we move towards needing efficient Light Emitting Diodes (LEDs) for displays. Key to developing better displays is the advancement of strategies for rationally designing emissive materials that are tunable and efficient. We report a series of emissive metal-organic frameworks (MOFs) generated using BUT-10 (BUT: Beijing University of Technology) that emits green light with λ_{max} at 525 nm. Post-synthetic reduction of the ketone on the fluorenone ligand in BUT-10 generates new materials, BUT-10-M and BUT-10-R. The emission for BUT-10-R is hypsochromically-shifted by 113 nm. Multivariate BUT-10-M structures demonstrate emission with two maxima corresponding to the emission of both fluorenol and fluorenone moieties present in their structures. Our study represents a novel post-synthetic ligand reduction strategy for producing emissive MOFs with tunable emission ranging from green, white-blue to deep blue.

Introduction

Materials with tunable emission are desirable for generating sensors and optical devices.[1] These materials emit color depending on their optoelectronic properties. Their band gap is a key predictor of the emitted color since fluorescence emission is based on the energy difference between the ground state and excited state.[2] With careful design, it is possible to alter the structure of a material, which in turn can emit a different color. For example, with aggregation-induced fluorescence, a molecule with weak fluorescence becomes strongly fluorescent when trapped in an aggregated state. Aggregation reduces non-radiative decay pathways and thus increases the fluorescent intensity.[3] Slight shifts in the emitted color can also occur with increased aggregation.[3b] Mechanical strain can also be used to alter the emission of crystalline compounds,[4] mechanical stress causes most crystals to collapse, resulting in a change in their structure and, thus emission.[5] Another factor that can impact the luminescent properties of materials is the way the crystal structure packs. Studies have shown that changing atomic arrangement within a crystal structure result in changes in their luminescence.[6] For example, Vaganova et al. found that structures that had increased π-interactions in their arrangement resulted in a bathochromic shift in emitted wavelength in 18-crown-6-ethers with co-crystals.[7] Other types of structural changes can also result in changes in emitted colors. For example, iridium (III) complexes were found to isomerize between *fac* and *mer* conformations using acids and bases. The *fac* isomer exhibited green emission, while the *mer* isomer exhibited an orange emission.[8] Additionally, Bauer et al. demonstrated that two extended framework structures composed of the same ligand and metal node could crystalize into a 2-dimensional or 3-dimensional structure.[6d] Fluorescent emission changed significantly between the 2-dimensional structure (blue emission) and the 3-dimensional structures (purple/blue emission), indicating that the local coordination and proximity of the ligands could be altered to tune the fluorescence of the material.[6d]

Metal-organic frameworks (MOFs) are materials made of inorganic clusters and organic ligands arranged in 3-dimensions.[9] Due to their versatile structures, crystallinity, and porosity,[2] MOFs can act as sensors[1,10] and exhibit guest molecule-induced changes in luminescence.[11] Most MOFs reported in the literature are comprised of a single organic ligand and metal ion; it has been shown that the generation of multivariate- (MTV-) MOFs can dramatically alter and/or improve their properties.[12] MTV-MOFs combine linkers with the same length and connectivity but with different functional groups with one or more metal centers, thus greatly expanding the library of possible structures.[9] There have been several studies investigating MTV-MOFs for their luminescent and sensing capabilities.[13] Most studies on luminescent MTV-MOF focus either on altering

[*] K. T. Smith, N.-C. Chiu, P. Jumrusprasert, K. C. Stylianou
Materials Discovery Laboratory (MaD Lab),
Oregon State University
Corvallis, OR 97331 (USA)
E-mail: kyriakos.stylianou@oregonstate.edu
K. T. Smith, K. Hunter, N.-C. Chiu, T. J. Zuehlsdorff, K. C. Stylianou
Department of Chemistry, Oregon State University
Corvallis, OR 97331 (USA)
H. Zhuang, J. A. Reimer
Department of Chemical and Biomolecular Engineering,
University of California
Berkeley, CA 94720 (USA)
P. Jumrusprasert
Chulalongkorn University
Bangkok, 10330 (Thailand)
W. F. Stickle
Hewlett-Packard Co.
1000 NE Circle Blvd., Corvallis, OR 97330 (USA)

the linkers or the metals in the MOF. For example, Jiang et al. created a series of MTV-MOFs that had two linkers [1,1′:4′,1″-terphenyl]-4,4″-dicarboxylic acid (H_2TPDC) and 4,4′-(benzo[c][1,2,5]-thiadiazole-4-7-diyl)dibenzoic acid (H_2BTDD) in different ratios to isolate the luminescent ligands within the MOF.[13c] This greatly enhanced the quantum yield of the material. Alternatively, researchers can mix different lanthanides in a MOF structure to tune the properties of the structure.[14] Combinations of both strategies are also feasible.[14]

While most MTV-MOFs are synthesized by pre-mixing metals and ligands, post-synthetic modification is an attractive strategy for forming MTV-MOFs.[15] Post-synthetic modification of MOFs allows for forming MOFs that cannot be synthesized otherwise.[16] Depending on the orientation and functionality of the ligands in MTV-MOFs, novel properties can emerge. One tool that has seen little use in creating MTV-MOFs is the post-synthetic reduction of key functional groups, such as ketones or aldehydes, to alcohols. Herein, we report the post-synthetic modification of a porous 3-dimensional MOF, BUT-10 (BUT: Beijing University of Technology), via reduction of the 9-fluorenone-2,7-dicarboxylic acid (FDC=O) ligand through its ketone group, resulting in MTV-MOFs with unique emission properties. FDC=O is from a class of promising luminescent ketones with applications in photoluminescent devices.[17] Reduction of FDC=O leads to the generation of FDC–OH (fluorenol containing an alcohol group), which disrupts the conjugated π system of BUT-10 (Figure 1a). Disrupting the π system results in a hypsochromic emission for the MOF material. BUT-10 can be post-synthetically modified to BUT-10-M containing both FDC=O and FDC–OH ligands. Our post-synthetic reduction strategy allows; i) to generate a MOF (with FDC–OH) that might be challenging to be synthesized; ii) to control the reduction conditions and generate MTV-MOFs with both FDC=O and FDC–OH in differing ratios and thus their emission color can be tuned; iii) the structural backbone of BUT-10 is not altered upon reduction of the ketone, allowing FDC=O and FDC–OH to share a BUT-10 crystal structure and thus be easily compared to each other.

Results and Discussion

BUT-10 was synthesized following literature procedures.[18] Zirconium (IV) chloride and 9-fluorenone-2,7-dicarboxylic acid (FDC=O) were combined in DMF and heated at 120 °C for 48 hours. Yellow/orange crystals are collected via gravity filtration. The powder is then washed with DMF, followed by acetone. The BUT-10 structure crystallizes in cubic P*a*-3 space group with 26.5 Å edge lengths with CCDC deposition

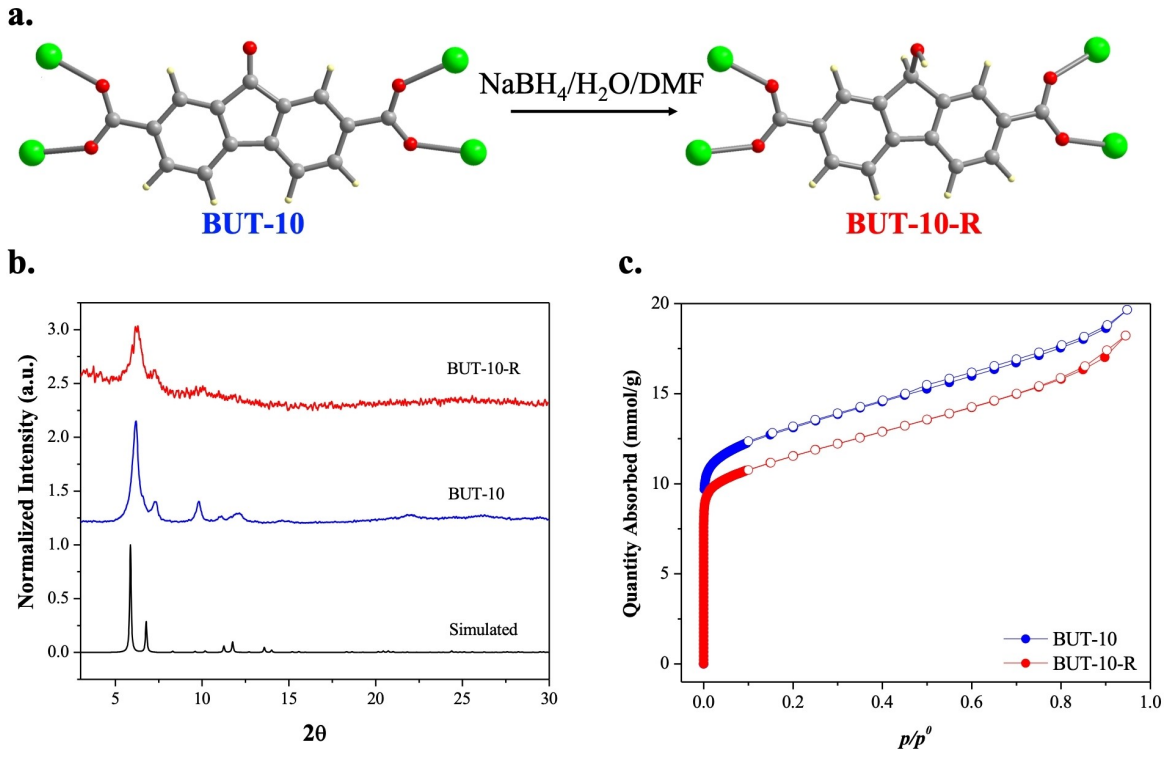

Figure 1. a) Schematic representation of the ligand reduction in BUT-10 with $NaBH_4$—the targeted ketone functional group of fluorenone, is reduced to an alcohol, the fluorenol. b) The PXRD pattern of BUT-10 (blue) is in excellent agreement with the simulated pattern confirming the synthesis of pure BUT-10. The pattern for BUT-10-R (red) shows the retention of the structure but a loss in crystallinity after reduction in aqueous/DMF $NaBH_4$ solution for 24 hours. c) Nitrogen isotherms for BUT-10 (blue) and BUT-10-R (red) demonstrate that BUT-10-R has a slight decrease in quantity absorbed compared to BUT-10 and is thought to be due to the slight loss of its crystallinity.

number 1002103. Hexanuclear $[Zr_6O_4(OH)_4]$ building units construct BUT-10 with twelve FDC=O ligands linking the metal clusters to form the 3-dimensional porous framework. Powder X-Ray Diffraction (PXRD) (Figure 1b) patterns confirm that BUT-10 can be synthesized as a pure phase. Fourier Transform Infrared Spectroscopy (FT-IR) characterization showed successful incorporation of the ligand to BUT-10, with key stretches at 1660 cm^{-1} attributed to the conjugated ketones in BUT-10 (Figure S1). Further characterization of BUT-10 included thermogravimetric analysis (TGA) (Figure S2). Three dips in the weight percent can be seen in the TGA; first, a loss of 24.7% before 100 °C, is attributed to the removal of water guest molecules within the pores. The second loss occurs between 100 °C and 200 °C, which is attributed to the removal of DMF guest molecules, and the third loss occurs at 500 °C when the MOF decomposes entirely. Through nitrogen sorption isotherms, we calculated the Brunauer–Emmett–Teller (BET) surface area of the activated BUT-10 is 1090 $m^2 g^{-1}$ (Figure 1c).[18]

The BUT-10 structure can be altered by reducing the FDC ligand at the FDC=O position to create FDC–OH-based ligands following the Scheme shown in Figure 1a. The resulting MOFs, called BUT-10-R and BUT-10-M (R: reduced, FDC–OH; M: multivariate (mixed ligands)), either have structures fully comprised of reduced FDC–OH ligands or have a mixture of FDC–OH and FDC=O ligands respectively. These structures can be generated by immersion of BUT-10 in DMF and deionized (DI) H_2O solution with sodium borohydride ($NaBH_4$). The immersion of BUT-10 in this solution for different times yields BUT-10-M or BUT-10-R. PXRD of the samples generated at different time points confirm that their crystallinity is lost to a significant degree (the peak broadening often occurs due to a decrease in crystal size, Figure S3). Still, their structural backbone is retained as confirmed by FT-IR, TGA, BET surface area and solid state (ss) ^{13}C NMR spectra. FT-IR confirmed that reduction occurred between BUT-10 and BUT-10-M/BUT-10-R (Figure S4). The TGA profile of BUT-10-R demonstrated no loss in thermal stability compared to BUT-10 (Figure S5). Nitrogen sorption isotherms of BUT-10-R give a BET surface area of 952 $m^2 g^{-1}$, which is slightly lower compared to BUT-10 (Figure 1c). Therefore, the pores have not been collapsed, indicating that the BUT-10 structural architecture is retained.

Solid-state (ss) ^{13}C NMR was performed to complement the characterization of BUT-10, BUT-10-R, and BUT-10-M10 and gain insights into the changes in these structures (Figures 2 and S6). Solid-state ^{13}C NMR on BUT-10 revealed that the peak at 191.57 ppm corresponds to the carbonyl carbon of the ketone. The rest of the peaks are associated with carbons within the benzene ring and result from the symmetry of the ligand. The peak at 169.49 ppm is associated with carboxylate-derived carbons. Additional peaks at 162.20, 35.36, and 30.03 ppm correspond to DMF guest molecules trapped in the pores of BUT-10. The ss ^{13}C NMR of BUT-10-R shows that the peak at 191.57 ppm is absent, and instead, there is a new peak at 73.24 ppm that corresponds to the benzylic carbon of the alcohol. This indicates that the FDC=O ligand in BUT-10 has been

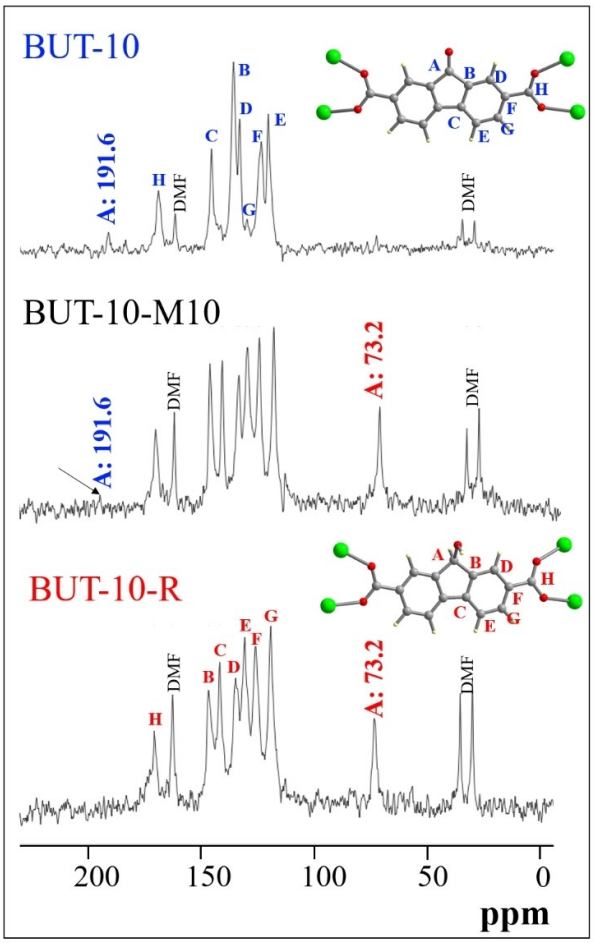

Figure 2. Solid state ^{13}C NMR spectra of BUT-10 (top), BUT-10-M10 (middle), and BUT-10-R (bottom). Assignments of the aromatic carbons are shown on the structure (Tables S1–S3). The key feature of the top spectrum (A: 191.6 ppm) shows that BUT-10 has a carbonyl carbon corresponding to the ketone group of FDC=O. The middle spectrum shows peaks at 191.6 and 73.2 ppm, indicating that both ketone and alcohol are present within the BUT-10-M8.5 structure. Finally, the bottom spectrum corresponds to BUT-10-R, with only the key feature at 73.2 ppm, corresponding to the allylic carbon.

reduced to FDC–OH in BUT-10-R. The rest of the peaks can all be associated with the expected carbon shifts of the benzene ring and carboxylic acid of the MOF (Tables S1–S3). The ss ^{13}C NMR spectra show that the MOF undergoes reduction to the point that the FDC=O cannot be seen in the NMR while still retaining the rest of the structure. Finally, the ss ^{13}C NMR spectrum of the BUT-10-M10 shows the presence of both BUT-10 and BUT-10-R structures. First, we can clearly see the presence of FDC–OH at 73.24 ppm. A minor peak at 191.57 ppm is also visible, suggesting that the FDC=O ligand is still present in the structure. Additionally, ^{1}H NMR of digested MOF samples ($\approx$1 mg of MOF digested in a highly concentrated base (NaOD) for a few minutes) provide a relative ratio of

FDC=O to FDC–OH for BUT-10-M6.5 and BUT-10-M8.5. Using the integration values for peaks associated with FDC=O and FDC–OH, we found that BUT-10-M6.5 had a ratio of 1:14 while BUT-10-M8.5 had a ratio of 1:15 (Figure S7). BUT-10 and BUT-10-R only had protons associated with FDC=O and FDC–OH and therefore no ratios could be calculated. Elemental analysis was performed confirmed the full reduction of BUT-10-R and partial reduction of BUT-10-M6.5 (Table S4). Together, we can see that reduction time does result in a relative chemical change between the two samples. Additionally, FT-IR spectra revealed a shift associated to conjugated ketones (at 1680–1660 cm^{-1}) in the BUT-10-M10, confirming that the ketone is still present in the BUT-10-M10 structure.

After confirming the structure of both BUT-10 and BUT-10-R, X-ray Photoelectron Spectroscopy (XPS) was performed to analyze their structures (Figures S8 and S9). From this data, we could determine the presence of atoms within the material and gain insights into the oxidation state of Zr^{IV}. BUT-10, and BUT-10-R have two peaks for the zirconium 3*d* orbital at the same binding energy (Figure S10). If Zr^{IV} was reduced to Zr^{III}, the binding energies would shift to lower binding energies. Therefore, it can be concluded that the reduction in the MOF is happening to the ligand alone. Sodium and boron were present in the spectrum of BUT-10-R since the reducing agent was not removed from the pores.

We examined the electronic structure of both BUT-10 and BUT-10-R to determine their structure change upon reduction of the FDC=O to FDC–OH. Reflectance data on both MOFs was taken and converted to Kubelka–Munk (KM), shown in Figure 3a. BUT-10 shows a sharp absorbance at 403 nm, whereas BUT-10-R has its first absorption peak at 325 nm. From the KM plots, Tauc plots determined the energy of the band gap (Figure S11). Both BUT-10 and BUT-10-R are converted into Tauc plots using the direct band gap equation.[19] From these plots, BUT-10 has a band gap of 2.48 eV. Using XPS, we determined that the valence band (VB) of BUT-10 is 3.53 eV. Using the equation of $E_{cb}=E_{vb}-E_g$ (where E_{cb} is the energy of the conduction

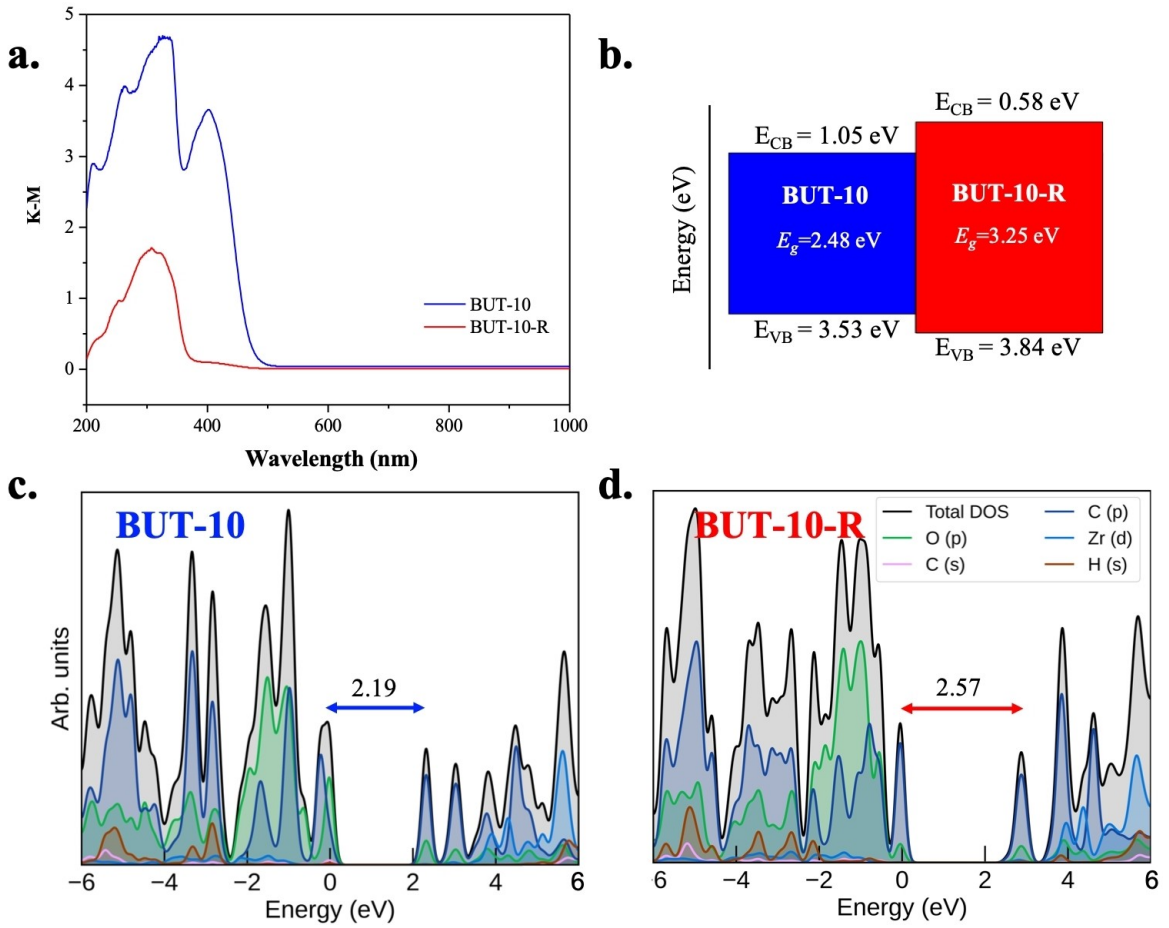

Figure 3. a) The absorption spectra of BUT-10 (blue) and BUT-10-R (red) were generated using the Kubelka–Munk (KM) function on the solid-state reflectance of the powder. b) The band gap diagram of BUT-10 (blue, left) and BUT-10-R (red, right) shows the broadening of the band gap and the shift in both the valence band (VB) and conduction band (CB). c), d) PDOS of BUT-10 and BUT-10-R generated through simulations showing the band gap; the trend seen with the computationally-derived band gaps is in agreement with our experimental results.

band, E_{vb} is the energy of the valence band, and E_g is the band gap energy), we can calculate the energy of the conduction band (CB) for BUT-10 to be 1.05 eV. BUT-10-R was found to have a band gap of 3.25 eV, a valence band of 3.82 eV, and a conduction band of 0.576 eV. A comparison of the band gaps is shown in Figure 3b, where the increasing size of the gap is shown to scale. For reference, GaN has a comparable band gap between 3.2 and 3.5 eV.[20]

The effects of substituting FDC=O with FDC–OH on the electronic structure of BUT-10 were explored computationally using density-functional theory (DFT). The smallest primitive cell of BUT-10 has 696 atoms, and in BUT-10-R, this increases to 744 atoms. Systems of this size can become challenging to correctly model using traditional cubic scaling DFT codes, so we employed the linear-scaling electronic structure code ONETEP[21] for all calculations of solid-state properties and geometries.[21a] The geometries of six different cells were minimized without symmetry constraints and at fixed unit cell dimensions: BUT-10, BUT-10 with a single FDC=O replaced by an FDC–OH, BUT-10-R, BUT-10-R with a single FDC–OH replaced by an FDC=O, BUT-10-M where the ligand sites were a distributed mixture of 50 % FDC=O and 50 % FDC–OH, and BUT-10-M where the cell was divided into two halves with each having only FDC=O or only FDC–OH (Figure 4, Figure S12). Using these calculations, we can analyze the band gap, localization of the VB and CB wavefunctions, the projected density of states (PDOS), and the relative total energies of the two BUT-10-M cells (Figure 3c and d). The band gaps calculated from DFT in this work (see Table S6) are underestimates of the band gaps calculated from experimental data, but they follow the same trend: BUT-10-R has a larger band gap than BUT-10 (Figure 3c and d). We attribute the difference in DFT and experimental values for the band gap to the semi-local nature of the PBE functional; semi-local exchange-correlation functionals like PBE are well known to underestimated band gaps in solid state calculations, but follow the same trends as experimental data, which is the case for

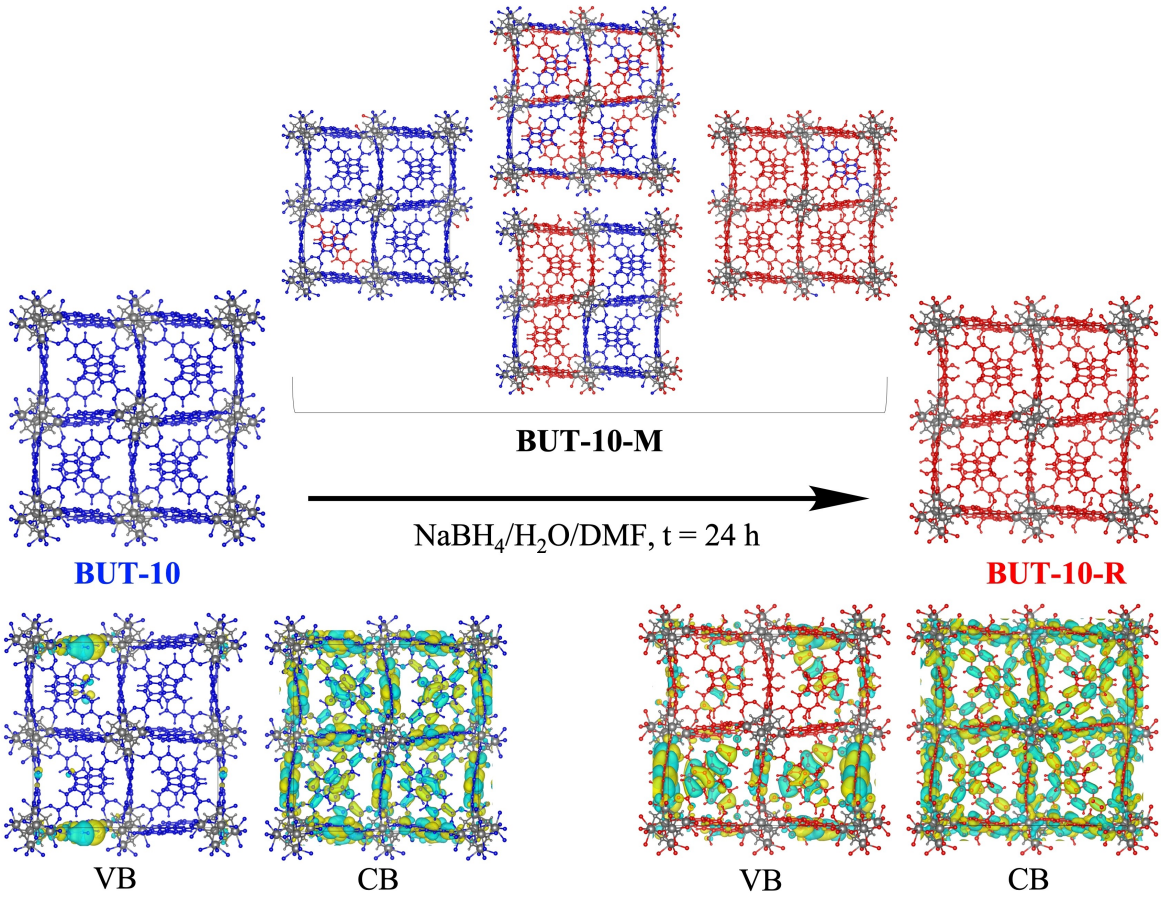

Figure 4. Computationally derived unit cell of BUT-10 as it undergoes reduction. The left BUT-10 structure (blue) shows fluorenone (ketone, FDC=O) ligands with their corresponding VB and CB beneath. Middle structures show different possible configurations of the fluorenol (red, FDC–OH) and fluorenone moieties in BUT-10-M with an increasing reduction. From left to right: a single defect of FDC–OH added to BUT-10-M, a 50–50 mixture of FDC=O and FDC–OH dispersed through the cell (top) or in layers (bottom), and a single defect of FDC=O added to BUT-10-M. The BUT-10-R structure is shown on the right, with their corresponding VB and CB on the bottom. The first VB of BUT-10 is mostly localized on a single ligand, while the first VB of BUT-10-R is more delocalized with density on several ligands. The first CB of both BUT-10 and BUT-10-R are delocalized across all ligands, but the first CB of BUT-10-R is additionally delocalized onto the Zr atoms.

our calculations.[22] Notable in these data is the dramatic change in the calculated band gap when BUT-10-R is given a single defect of FDC=O, the reason for which is illustrated by the VB and CB orbitals (Figures 4, S13, and S14). In BUT-10, the highest VB is localized on a single FDC=O ligand, while the lowest CB is delocalized across all ligands, though without significant density on the $Zr_6O_4(OH)_4$ nodes. As more FDC–OH are substituted in BUT-10, the VB wavefunction becomes more delocalized, and shifts to predominantly on the FDC–OH ligands, but even in BUT-10-R, the highest VB only spans half of the ligands. The CB follows an opposite trend: as fewer FDC=O ligands are present, it remains localized across all of them until that results in it being localized on the single defect in substituted BUT-10-R. In the cell of purely FDC–OH, the CB again becomes delocalized across all ligands, but there are also contributions from the Zr *d*-orbitals. BUT-10 and BUT-10-R have been demonstrated to have different optoelectronic properties (i.e. band gap) therefore we hypothesized that the fluorescence spectra of the material would have a corresponding shift, with BUT-10-R having a lower wavelength (higher energy) of emission than BUT-10. To explore this, we investigated the solid-state emission of BUT-10 and its derivatives.

All emission spectra discussed below were excited at 325 nm. The emission spectrum of BUT-10 resembles the emission spectrum of the protonated FDC=O ligand (λ_{max} = 508 nm) but is red-shifted by 17 nm (Figure S15). Often, incorporating a ligand into a MOF can result in a shift in λ_{max}, which was seen in a small shift in BUT-10 due to the isolation of the ligands preventing any interactions between them, and ligand-to-metal-charge transfer (LMCT). Additionally, incorporating the FDC=O into the 3-dimensional MOF lead to the separation of the ligands and reducing non-radiative decay pathways, resulting in enhanced fluorescence.[2] BUT-10 has a quantum yield of 5.2% (Table 1). The absence of the Zr nodes from the frontier orbitals and PDOS of BUT-10 agree with the experimental observation that there is little change in the fluorescence of FDC=O when placed in the MOF environment; for example, the nature of the excitons in BUT-10 are generally similar to the excitons generated by the ligands in solution, do not couple significantly to the Zr nodes, and continue to produce green. Reduction for 6.5 hours produced an MTV-MOF: BUT-10-M6.5. Due to the presence of both FDC–OH and FDC=O ligands in the structure, we observed two emission maxima (Figure 5a). Traditionally, it is challenging to generate materials with multiple emissions from a single excitation wavelength; other MOFs have obtained similar emissions, but generally, this can be done through a combination of different emissive metals or ligands that are incorporated via synthesis rather than the direct generation

Table 1: Optical values for BUT-10 and its derivatives. The λ_{max} and their intensities are given as the highest intensity wavelength in the given materials spectra, where as $\lambda_{max'}$ and their intensities are the second highest intensity wavelength in the materials spectra.

Material	λ_{max} [nm]	Intensity at λ_{max}	$\lambda_{max'}$ [nm]	Intensity at $\lambda_{max'}$	Quantum Yield (QY)	CIE
BUT-10	525	5141	n/a	n/a	5.2%	(0.314, 0.478)
BUT-10-M6.5	505	7893	411	4715	6.0%	(0.260, 0.371)
BUT-10-M-8.5	411	4182	505	4052	5.0%	(0.267, 0.335)
BUT-10-R	412	26080	n/a	n/a	8.0%	(0.194, 0.171)

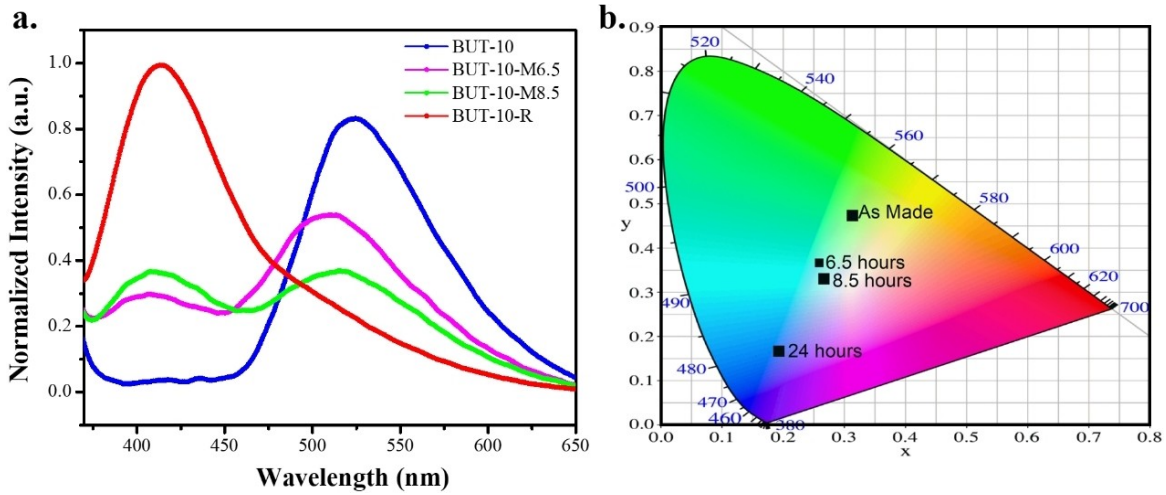

Figure 5. a) Fluorescence emission spectra of four materials excited at 325 nm: BUT-10 (blue), BUT-10-M6.5 (magenta), BUT-10-M8.5 (green), and BUT-10-R (red). BUT-10 and BUT-10-R show strong, single maxima emission, while BUT-10-M6.5 and BUT-10-M8.5 show two maxima from a single excitation wavelength. b) The calculated CIE 1931 coordinates of BUT-10 (as made), BUT-10-M6.5 (6.5 hours), BUT-10-M8.5 (8.5 hours), and BUT-10-R (24 hours) show the change in color as a result of increased reduction time.

of the new ligand in the MOF crystal.[23] The emission with λ_{max} at 505 nm is associated with the fluorescence of the FDC=O, though it is blue-shifted compared to the emission of BUT-10. Likewise, the emission with λ_{max} at 412 nm occurs from the FDC–OH and lines up well with the fully reduced (BUT-10-R) material. In terms of intensity, BUT-10-M6.5 has a more intense 505 nm peak than the 412 nm peak. Based on this, we can use the emission wavelength as a fingerprint for the associated functionality (i.e., 412 nm is associated with FDC–OH functionality, and 505 nm is associated with FDC=O functionality). BUT-10-M6.5 has a quantum yield of 6.0 %, slightly higher than BUT-10. Another MTV-MOF, BUT-10-M8.5, was produced by reducing FDC=O in BUT-10 for 8.5 hours, and we can also see the same two emission maxima. They are in the same locations as BUT-10-M6.5, however, the peak at 412 nm has a stronger intensity than the 505 nm peak. The change in intensity, coupled with the increase in time of the reduction, indicates that as reduction occurs, the intensity of the 505 nm peak will decrease, and the intensity of the 412 nm peak will increase. This observation aligns with expectations that as the concentration of FDC=O decreases, so will the emission due to that ligand, though the relationship very likely non-linear. BUT-10-M8.5 has a quantum yield of 5.0 %. In Figure 5, it appears that the fluorescence of BUT-10-M is not a linear combination of the spectra of BUT-10 and BUT-10-R. The intensity of the lower energy peak decreases significantly, going from BUT-10-M6.5 to BUT-10-M8.5, while the intensity of the higher energy peak increases only slightly. As a control, we submerged BUT-10 in both DMF and water and collected fluorescence spectra of the material after being filtered; the emission of BUT-10 after immersion in DMF was identical with that of BUT-10, but after submerging in water, we observed a red shift in the emission indicating that solvent effects did not contribute to the hypsochromic shifts seen in the reduced MTV-MOFs (Figure S16).[24] Additionally, excitation spectra were taken of all four samples for both 412 and 525 nm emission. When the emission wavelength is set to 525 nm, and the excitation range is scanned, we can see that BUT-10 is blue-shifted from the ligand. As BUT-10 is reduced to BUT-10-M6.5, BUT-10-M8.5, and BUT-10-R the intensity of λ_{max} decreases, but the λ_{max} does not shift. This indicates that the emission seen at 525 nm is derived from the FDC=O ligands in the MOF that does not get reduced (Figure S17). Similarly, we collected the excitation spectra with the emission wavelength set at 412 nm. In this case, BUT-10 and FDC=O do not show any intensity. Only the reduced ligand-based MOFs emit in this region and have similar excitation spectra (Figures S17–S18). This helps to corroborate that BUT-10-M6.5, BUT-10-M8.5, and BUT-10-R are emitting from the same luminescent center, and a luminescent center that is not FDC=O.

Several effects could result in reduced intensity of the emission with λ_{max} of 411 nm in BUT-10-M, but the most are likely (i) resonance energy transfer (RET), where Förster type transfer via transition dipole moment coupling and radiative transfer via photon recycling[25] are considered together[26] and (ii) exciton transfer via the wavefunction overlap between neighboring FDC–OH ligands in the CB of BUT-10-R and FDC–OH rich regions of BUT-10-M.[25] The possibility of an indirect transfer of an exciton via a RET process is particularly favorable in the case of BUT-10-M, as the emission peak of BUT-10-R and the lowest energy absorption peak of BUT-10 have significant overlap in the 400–500 nm region, and the density of both ligands is much higher compared with what might be observed for the ligands free in solution, which helps to overcome the distance dependent component of RET. In line with the possibility of wavefunction overlap playing a role in quenching emission from FDC–OH is the observation that the ligand's frontier states are energetically near those of the Zr nodes, creating an additional path for exciton transfer among FDC–OH ligands (Figure S19f). Therefore, it is possible for an exciton formed on an FDC–OH ligand in BUT-10-M to move towards an FDC=O ligand that is not nearby before jumping to FDC=O via FRET and subsequently emitting a lower energy photon. To determine how significant the distance dependence of RET would be, we explored two ways that FDC=O ligands could be converted to FDC–OH as a reduction reaction proceeds in BUT-10-M: either the FDC–OH ligands can congregate in a separate phase, or the FDC–OH ligands can form semi-randomly throughout the cell (Figure 4). To investigate whether a mixed phase or separate phases are more likely we compare the total energies of our optimized BUT-10-M cells, without relaxing the unit cell parameters, such comparisons are only qualitative, but the difference in total energy between the two configurations is 5.8 kJ mol^{-1} (2.3 × kT at 300 K), with the unit cell with separate FDC=O and FDC–OH layers being the more stable. From this, we can predict that as the FDC=O→FDC–OH reduction reaction proceeds in BUT-10, regions of only FDC–OH will begin to form, trapping the excitons too far from an FDC=O to move there before emitting without nonradiative transfer due to wavefunction overlap. Therefore, although RET will play a role in the quenching of FDC–OH emission, it is amplified but non-radiative pathways in BUT-10-M, likely result from a mixture of effects, with the remaining blue emissions resulting from the finite lifetime of the excited state.

The λ_{max} for BUT-10-R is seen only at 412 nm with a long tail extending to 600 nm. This interesting feature could be due to a small amount of residual FDC=O in structure or vibrational energy bands.[27] BUT-10-R has a quantum yield of 8.0 %, higher than the other three MOFs. For comparison, a MOF using a mixed linker strategy, JLNU-7, was reported to have 11 %.[14] In agreement with the frontier orbitals, the PDOS (Figure S19) show that there is very little contribution to the states near the band gap from the Zr, but the band that becomes the CB in BUT-10-R does have some contribution from Zr *d*-orbitals. The visualizations of the CB show that the oxygen in the Zr nodes also does not contribute significantly to the CB (Figure S14). Compared to BUT-10, the excited state of BUT-10-R does mix with Zr *d*-orbitals providing increased delocalization.

Additionally, Figure 5b shows the calculated CIE 1931 coordinates for each of the four materials described in this study.[28] CIE coordinates are an objective measure of the

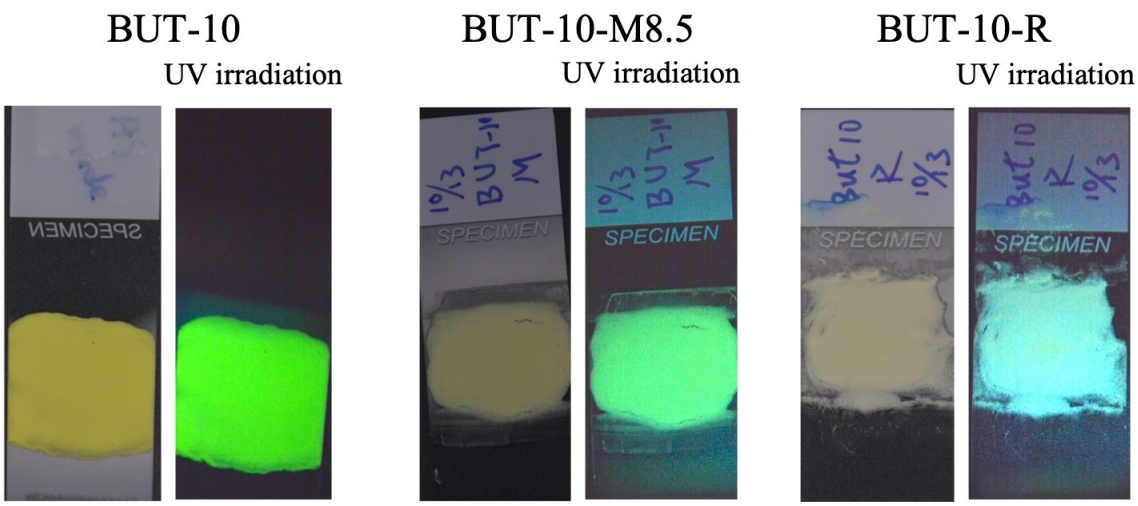

Figure 6. Thin films of BUT-10 (left), BUT-10-M8.5 (middle), and BUT-10-R (right) were integrated onto microscope slides using the doctor blade method. Each film was irradiated using a handheld UV light to demonstrate that the materials emit visibly different colors, with BUT-10 emitting a green color and BUT-10-R being a blue emissive material. BUT-10-M8.5 thin film is somewhere between a pale green-blue color. These films are created with a suspension of PVDF, making their colors shift slightly from the fluorescence shown in the pure powder form of the materials.

material's color related to display technologies. By using these coordinates, we can assess the emission color for our MOFs with more precision. BUT-10 has coordinates of (0.3137, 0.4775), placing it in the green-yellow emission range. Comparatively, BUT-10-M6.5 and BUT-10-M8.5 have coordinates of (0.2595, 0.3710) and (0.2674, 0.3347), respectively, placing them near the white-blue range in their emission. BUT-10-R has a deep blue emission of (0.1938, 0.1707). Other MOFs have been designed to achieve blue emission with Cs-PeMOF having a quantum yield of 15 %,[29] and a Zn-based MOF with lanthanides encapsulated in it, MOF-1, was reported to have efficient blue light emission with a quantum yield of 2.5 %.[30] Most of the blue-emitting materials in the literature rely on lanthanides, layered structures, or blue-emitting guest molecules to achieve their blue light. Our strategy highlights the impact of MTV-MOFs to achieve unique color emissions through the mixture of FDC=O and FDC–OH ligands in a single material. By tuning the ligand ratios (via variations in the reduction time), the shade of the blue-emitting MOF can be finely controlled.

The tunable color emissions prompted us to further investigate the creation of MOF thin films. To demonstrate the potential of BUT-10, BUT-10-M, and BUT-10-R to be integrated into a downward conversion light-emitting device, we developed thin films of the MOFs.[14] Thin films were created by making a suspension of BUT-10 in 5 % Polyvinylidene fluoride (PVDF) in N-methyl-2-pyrrolidone (NMP). Once a well-distributed suspension was made, the suspension was coated onto a microscope slide using the Doctor Blade Method. Figure 6 shows photos of all three films under UV light, demonstrating how the materials fluoresce different colors based on their reduction time. Qualitatively, the change in the color hews closely to the results of the fluorescence spectra, with increasing reduction times resulting in a stronger blue color.

Conclusion

In summary, we have demonstrated a successful method for generating MOFs with tunable emission by using a one-step reduction scheme to convert FDC=O in BUT-10 to FDC–OH in BUT-10-R. This has a corresponding hypsochromic shift of 113 nm (576 meV) going from BUT-10 to BUT-10-R. The quantum yield of the BUT-10-R is 3 % higher compared to BUT-10. By reducing BUT-10 for less than 24 hours, BUT-10-M-MTV-MOFs, with both FDC=O and FDC–OH ligands were generated. BUT-10-M structures demonstrate dual-emission from a single excitation wavelength with two maxima. These MOFs showed a change in color from green to blue with CIE coordinates of (0.3137, 0.4775), (0.2595, 0.3710), (0.2674, 0.3347), and (0.1938, 0.1707) for BUT-10, BUT-10-M6.5, BUT-10-M8.5, and BUT-10-R respectively. The dual-emission was shown to not be a direct linear combination of BUT-10 and BUT-10-R, indicating that additional mechanisms, namely RET and non-radiative transfer, are at play in the multivariate structures. Our work sheds light on the interface of structure and luminescence of functional MOFs and presents a new way to create new MOFs with tunable emissions.

Supporting Information

Experimental methods, emission profiles for all MOFs, computational methods, and analysis are provided in the Supporting Information.

Acknowledgements

K.C.S. thanks the Department of Chemistry at Oregon State University (OSU) for support through start-up funding and the College of Science SciRIS-II grant (2021). T.J.Z. thanks the Department of Chemistry at Oregon State University (OSU) for support through start-up funding. K.T.S and N.C.C. acknowledge support from the Department of Chemistry for their Benedict Award and David P. & Clara B. Shoemaker Graduate fellowships, respectively. K.T.S. receives support from a scholar award funded by the ARCS Foundation Oregon. K.C.S. thanks Marilyn and Brian Kleiner for their generous support of this project through their donor-advised funds. The authors thank Casey Simons for collecting some of the NMR spectra shown in this work.

Conflict of Interest

The authors declare no conflict of interest.

Data Availability Statement

The data that support the findings of this study are available from the corresponding author upon reasonable request.

Keywords: Blue-Light · Dual-Emission · Hypsochromic · Multivariate-MOFs · Post-Synthetic Modification

[1] F. M. Ebrahim, T. N. Nguyen, S. Shyshkanov, A. Gładysiak, P. Favre, A. Zacharia, G. Itskos, P. J. Dyson, K. C. Stylianou, *J. Am. Chem. Soc.* **2019**, *141*, 3052–3058.
[2] A. Karmakar, J. Li, *Chem. Commun.* **2022**, *58*, 10768–10788.
[3] a) L. Shen, C.-J. Yu, H.-F. Xie, N. Xu, H. Xu, Y.-L. Huang, C. Redshaw, X. Feng, Q.-L. Zhang, *Mater. Chem. Front.* **2022**, *6*, 2491–2498; b) P. Srujana, T. Gera, T. P. Radhakrishnan, *J. Mater. Chem. C* **2016**, *4*, 6510–6515; c) H.-Q. Yin, X.-Y. Wang, X.-B. Yin, *J. Am. Chem. Soc.* **2019**, *141*, 15166–15173.
[4] T. Seki, K. Sakurada, H. Ito, *Chem. Commun.* **2015**, *51*, 13933–13936.
[5] a) T. Seki, H. Ito, *Chem. Eur. J.* **2016**, *22*, 4322–4329; b) T. Seki, K. Sakurada, H. Ito, *Angew. Chem. Int. Ed.* **2013**, *52*, 12828–12832.
[6] a) J.-C. Dai, X.-T. Wu, Z.-Y. Fu, C.-P. Cui, S.-M. Hu, W.-X. Du, L.-M. Wu, H.-H. Zhang, R.-Q. Sun, *Inorg. Chem.* **2002**, *41*, 1391–1396; b) M. Głodek, S. Pawlędzio, A. Makal, D. Plażuk, *Chem. Eur. J.* **2019**, *25*, 13131–13145; c) D. Tchoń, D. Bowskill, I. Sugden, P. Piotrowski, A. Makal, *J. Mater. Chem. C* **2021**, *9*, 2491–2503; d) C. A. Bauer, T. V. Timofeeva, T. B. Settersten, B. D. Patterson, V. H. Liu, B. A. Simmons, M. D. Allendorf, *J. Am. Chem. Soc.* **2007**, *129*, 7136–7144.
[7] T. A. Vaganova, Y. V. Gatilov, E. Benassi, I. P. Chuikov, D. P. Pishchur, E. V. Malykhin, *CrystEngComm* **2019**, *21*, 5931–5946.
[8] A. Yu. Gitlina, F. Fadaei-Tirani, A. Ruggi, C. Plaice, K. Severin, *Chem. Sci.* **2022**, *13*, 10370–10374.
[9] H. Deng, C. J. Doonan, H. Furukawa, R. B. Ferreira, J. Towne, C. B. Knobler, B. Wang, O. M. Yaghi, *J. Sci.* **2010**, *327*, 846–850.
[10] a) C.-X. Chen, Y.-Y. Xiong, X. Zhong, P. C. Lan, Z.-W. Wei, H. Pan, P.-Y. Su, Y. Song, Y.-F. Chen, A. Nafady Sirajuddin, S. Ma, *Angew. Chem. Int. Ed.* **2022**, *61*, e202114071; b) S. Li, Y. G. Chung, C. M. Simon, R. Q. Snurr, *J. Phys. Chem. Lett.* **2017**, *8*, 6135–6141; c) W. Li, J. Wang, D. He, G. He, H. Chen, *J. Mol. Catal.* **2022**, *529*, 112520; d) A. Ma, H. Cong, H. Deng, *Green Energy Environ.* **2022**, *7*, 575–577; e) S. Patial, P. Raizada, V. Hasija, P. Singh, V. K. Thakur, V. H. Nguyen, *Mater. Today Energy Mater.* **2021**, *19*, 100589; f) L. Wang, L. Ren, X. Wang, X. Feng, J. Zhou, B. Wang, *ACS Appl. Mater. Interfaces* **2018**, *10*, 4750–4756; g) S.-L. Yang, G. Li, M.-Y. Guo, W.-S. Liu, R. Bu, E.-Q. Gao, *J. Am. Chem. Soc.* **2021**, *143*, 8838–8848; h) J.-M. Li, R. Li, X. Li, *CrystEngComm* **2018**, *20*, 4962–4972; i) M. Ko, A. Aykanat, M. K. Smith, K. A. Mirica, *Sensors* **2017**, *17*, 2192.
[11] P. L. Feng, K. Leong, M. D. Allendorf, *J. Chem. Soc. Dalton Trans.* **2012**, *41*, 8869–8877.
[12] a) J. Cornelio, T.-Y. Zhou, A. Alkaş, S. G. Telfer, *J. Am. Chem. Soc.* **2018**, *140*, 15470–15476; b) W. J. Newsome, S. Ayad, J. Cordova, E. W. Reinheimer, A. D. Campiglia, J. K. Harper, K. Hanson, F. J. Uribe-Romo, *J. Am. Chem. Soc.* **2019**, *141*, 11298–11303; c) S. Wu, D. Ren, K. Zhou, H.-L. Xia, X.-Y. Liu, X. Wang, J. Li, *J. Am. Chem. Soc.* **2021**, *143*, 10547–10552.
[13] a) Y. Jin, H. Lu, B. Yan, *Dyes Pigm.* **2021**, *194*, 109588; b) Y.-N. Zeng, H.-Q. Zheng, J.-F. Gu, G.-J. Cao, W.-E. Zhuang, J.-D. Lin, R. Cao, Z.-J. Lin, *Inorg. Chem.* **2019**, *58*, 13360–13369; c) Z. Jiang, H.-Q. Zheng, L. Guan, Y. Yang, Y. Cui, G. Qian, *J. Mater. Chem. C* **2022**, *10*, 10473–10479; d) Z. Jiang, H.-Q. Zheng, L. Guan, Y. Yang, Y. Cui, G. Qian, *J. Mater. Chem. C* **2022**, *10*, 1473–1479; e) C.-X. Chen, Q.-F. Qiu, M. Pan, C.-C. Cao, N.-X. Zhu, H.-P. Wang, J.-J. Jiang, Z.-W. Wei, C.-Y. Su, *Chem. Commun.* **2018**, *54*, 13666–13669; f) K. Talha Alamgir, N. Ahmed, L.-H. Xie, X. Zhang, J.-R. Li, *CrystEngComm* **2021**, *23*, 4923–4929.
[14] N.-C. Chiu, K. T. Smith, K. C. Stylianou, *Coord. Chem. Rev.* **2022**, *459*, 214441.
[15] L. R. Parent, M. S. Denny, J. P. Patterson, P. Abellan, Q. M. Ramasse, F. Paesani, S. M. Cohen, N. C. Gianneschi, *Microsc. Microanal. Microstruct.* **2018**, *24*, 1970–1971.
[16] S. M. Cohen, *J. Am. Chem. Soc.* **2017**, *139*, 2855–2863.
[17] X. Zhang, Y. Quan, Z. Cui, Q. Chen, J. Ding, J. Lu, *Eur. J. Org. Chem.* **2010**, 2295–2303.
[18] B. Wang, H. Huang, X.-L. Lv, Y. Xie, M. Li, J.-R. Li, *Inorg. Chem.* **2014**, *53*, 9254–9259.
[19] P. Makuła, M. Pacia, W. Macyk, *J. Phys. Chem. Lett.* **2018**, *9*, 6814–6817.
[20] P. Perlin, I. Gorczyca, T. Suski, P. Wisniewski, S. Lepkowski, N. Christensen, A. Svane, M. Hansen, S. Denbaars, B. Damilano, N. Grandjean, J. Massies, *Phys. Rev. B* **2001**, *64*, 115319.
[21] a) J. C. A. Prentice, J. Aarons, J. C. Womack, A. E. A. Allen, L. Andrinopoulos, L. Anton, R. A. Bell, A. Bhandari, G. A. Bramley, R. J. Charlton, R. J. Clements, D. J. Cole, G. Constantinescu, F. Corsetti, S. M. M. Dubois, K. K. B. Duff, J. M. Escartín, A. Greco, Q. Hill, L. P. Lee, E. Linscott, D. D. O'Regan, M. J. S. Phipps, L. E. Ratcliff, Á. R. Serrano, E. W. Tait, G. Teobaldi, V. Vitale, N. Yeung, T. J. Zuehlsdorff, J. Dziedzic, P. D. Haynes, N. D. M. Hine, A. A. Mostofi, M. C. Payne, C.-K. Skylaris, *Chem. Phys.* **2020**, *152*, 174111; b) C.-K. Skylaris, P. D. Haynes, A. A. Mostofi, M. C. Payne, *Chem. Phys.* **2005**, *122*, 084119.
[22] P. Borlido, J. Schmidt, A. W. Huran, F. Tran, M. A. L. Marques, S. Botti, *Npj Comput. Mater.* **2020**, *6*, 96.
[23] H.-Q. Yin, X.-B. Yin, *Acc. Chem. Res.* **2020**, *53*, 485–495.
[24] K. C. Stylianou, R. Heck, S. Y. Chong, J. Bacsa, J. T. A. Jones, Y. Z. Khimyak, D. Bradshaw, M. J. Rosseinsky, *J. Am. Chem. Soc.* **2010**, *132*, 4119–4130.

[25] C. Cho, Y.-W. Jang, S. Lee, Y. Vaynzof, M. Choi, J. H. Noh, K. Leo, *Sci. Adv.* **2021**, *7*, eabj1363.
[26] G. A. Jones, D. S. Bradshaw, *Front. Physiol. Front. Phys.* **2019**, *7*, 100.
[27] H. Xi, C.-X. Yuan, Y.-X. Li, Y. Liu, X.-T. Tao, *CrystEngComm* **2012**, *14*, 2087–2093.
[28] T. Smith, J. Guild, *Opt. Soc.* **1931**, *33*, 73.
[29] H. Tsai, H.-H. Huang, J. Watt, C.-H. Hou, J. Strzalka, J.-J. Shyue, L. Wang, W. Nie, *Adv. Sci. Lett.* **2022**, *9*, 2105850.
[30] W. Huang, F. Pan, Y. Liu, S. Huang, Y. Li, J. Yong, Y. Li, A. M. Kirillov, D. Wu, *Inorg. Chem.* **2017**, *56*, 6362–6370.

Manuscript received: February 11, 2023
Accepted manuscript online: March 16, 2023
Version of record online: ■■, ■■

Research Articles

Metal-Organic Frameworks

K. T. Smith, K. Hunter, N.-C. Chiu, H. Zhuang, P. Jumrusprasert, W. F. Stickle, J. A. Reimer, T. J. Zuehlsdorff, K. C. Stylianou* _____ **e202302123**

Hypsochromically-shifted Emission of Metal-organic Frameworks Generated through Post-synthetic Ligand Reduction

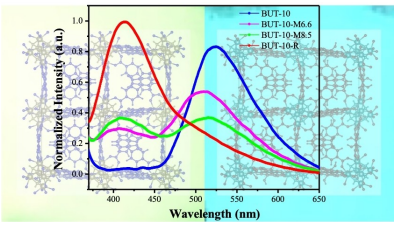

Post-synthetic ligand reduction in luminescent MOFs results in the generation of materials that can emit green, white-blue and deep blue light.

SPACE RESERVED FOR IMAGE AND LINK

Share your work on social media! *Angewandte Chemie* has added Twitter as a means to promote your article. Twitter is an online microblogging service that enables its users to send and read short messages and media, known as tweets. Please check the pre-written tweet in the galley proofs for accuracy. If you, your team, or institution have a Twitter account, please include its handle @username. Please use hashtags only for the most important keywords, such as #catalysis, #nanoparticles, or #proteindesign. The ToC picture and a link to your article will be added automatically, so the **tweet text must not exceed 250 characters**. This tweet will be posted on the journal's Twitter account (follow us @angew_chem) upon publication of your article in its final (possibly unpaginated) form. We recommend you to re-tweet it to alert more researchers about your publication, or to point it out to your institution's social media team.

Please check that the ORCID identifiers listed below are correct. We encourage all authors to provide an ORCID identifier for each coauthor. ORCID is a registry that provides researchers with a unique digital identifier. Some funding agencies recommend or even require the inclusion of ORCID IDs in all published articles, and authors should consult their funding agency guidelines for details. Registration is easy and free; for further information, see http://orcid.org/.

Kyle T. Smith
Kye Hunter
Nan-Chieh Chiu
Hao Zhuang
Peemapat Jumrusprasert
William F. Stickle
Jeffrey A. Reimer
Tim J. Zuehlsdorff
Kyriakos C. Stylianou http://orcid.org/0000-0003-1670-0020